ASTEROIDS

Hayabusa2 arrives at the carbonaceous asteroid 162173 Ryugu—A spinning top-shaped rubble pile

S. Watanabe[1,2]*, M. Hirabayashi[3], N. Hirata[4], Na. Hirata[5], R. Noguchi[2], Y. Shimaki[2], H. Ikeda[6], E. Tatsumi[7], M. Yoshikawa[2,8], S. Kikuchi[2], H. Yabuta[9], T. Nakamura[10], S. Tachibana[7,2], Y. Ishihara[2]†, T. Morota[1], K. Kitazato[4], N. Sakatani[2], K. Matsumoto[11,8], K. Wada[12], H. Senshu[12], C. Honda[4], T. Michikami[13], H. Takeuchi[2,8], T. Kouyama[14], R. Honda[15], S. Kameda[16], T. Fuse[17], H. Miyamoto[7], G. Komatsu[18,12], S. Sugita[7], T. Okada[2,7], N. Namiki[11,8], M. Arakawa[5], M. Ishiguro[19], M. Abe[2,8], R. Gaskell[20], E. Palmer[20], O. S. Barnouin[21], P. Michel[22], A. S. French[23], J. W. McMahon[23], D. J. Scheeres[23], P. A. Abell[24], Y. Yamamoto[2,8], S. Tanaka[2,8], K. Shirai[2], M. Matsuoka[2], M. Yamada[12], Y. Yokota[2,15], H. Suzuki[25], K. Yoshioka[7], Y. Cho[7], S. Tanaka[5], N. Nishikawa[5], T. Sugiyama[4], H. Kikuchi[7], R. Hemmi[7], T. Yamaguchi[2]‡, N. Ogawa[2], G. Ono[6], Y. Mimasu[2], K. Yoshikawa[6], T. Takahashi[2], Y. Takei[2], A. Fujii[2], C. Hirose[6], T. Iwata[2,8], M. Hayakawa[2], S. Hosoda[2], O. Mori[2], H. Sawada[2], T. Shimada[2], S. Soldini[2], H. Yano[2,8], R. Tsukizaki[2], M. Ozaki[2,8], Y. Iijima[2]§, K. Ogawa[5], M. Fujimoto[2], T.-M. Ho[26], A. Moussi[27], R. Jaumann[28], J.-P. Bibring[29], C. Krause[30], F. Terui[2], T. Saiki[2], S. Nakazawa[2], Y. Tsuda[2,8]

The Hayabusa2 spacecraft arrived at the near-Earth carbonaceous asteroid 162173 Ryugu in 2018. We present Hayabusa2 observations of Ryugu's shape, mass, and geomorphology. Ryugu has an oblate "spinning top" shape, with a prominent circular equatorial ridge. Its bulk density, 1.19 ± 0.02 grams per cubic centimeter, indicates a high-porosity (>50%) interior. Large surface boulders suggest a rubble-pile structure. Surface slope analysis shows Ryugu's shape may have been produced from having once spun at twice the current rate. Coupled with the observed global material homogeneity, this suggests that Ryugu was reshaped by centrifugally induced deformation during a period of rapid rotation. From these remote-sensing investigations, we identified a suitable sample collection site on the equatorial ridge.

Carbonaceous (or C-complex) asteroids are leftover debris from planet formation in the solar nebula. Studying their formation, evolution, and volatile content provides information on formation processes around the snow line—the boundary between the inner and outer Solar System (SS). Carbonaceous asteroids may have delivered water and organic materials to early Earth (*1*). The Hayabusa2 mission goal is to rendezvous with a carbonaceous asteroid and probe these issues by means of a combination of remote-sensing observations from the spacecraft, in situ surface measurements by deployed rovers and a lander, execution of an artificial impact experiment, and analyses of samples returned to Earth (*2*, *3*). The spacecraft was developed by the Japan Aerospace Exploration Agency (JAXA) as a successor to Hayabusa (*4*) and was launched by an H-IIA rocket on 3 December 2014. Its target is the near-Earth carbonaceous asteroid 162173 Ryugu (provisional designation 1999 JU_3). Hayabusa2 reached its target in June 2018; NASA's OSIRIS-REx spacecraft (*5*) reached another carbonaceous asteroid 101955 Bennu in December 2018.

After a 3.5-year cruise, a satellite search during approach to the asteroid detected no natural satellites >0.1 m within 100 km (*6*). Hayabusa2 arrived at the Home Position (HP), located at an altitude of ~20 km above Ryugu, on 27 June 2018 (*6*). The spacecraft did not enter into circumasteroid orbit but hovered at HP during the initial mapping phase. The remote-sensing instrument suite onboard Hayabusa2 includes the Optical Navigation Camera–Telescopic (ONC-T) with a wideband and seven narrowband filters (*7*, *8*), a Thermal Infrared Imager (TIR) (*9*), a Near-Infrared Spectrometer (NIRS3) (*10*), and a laser Light Detection and Ranging (LIDAR) system (*11*). Coordinated observations among these instruments (fig. S1) (*6*) enabled an initial assessment of Ryugu's general physical characteristics. The spectral data obtained with ONC-T and NIRS3 indicated that Ryugu is a Cb-type asteroid with a low geometric albedo of 4.5 ± 0.2% at 0.55 μm (*8*, *10*).

ONC-T images reveal geomorphological features that include the presence of numerous boulders on the surface (Fig. 1). From these images, we constructed global shape models with two different methods: stereophotoclinometry (SPC) (*12*) and the Structure-from-Motion (SfM) technique (*13*). These methods yielded shape models with polygon mesh resolutions of ~1 m. The two model topographies are in good agreement with each other (the standard deviation of height differences between them is ~1.5 m), except for around some boulders and in the polar regions (fig. S2) (*6*). The SfM-based shape model is shown in Fig. 2.

Ryugu's derived orbital and physical parameters are summarized in table S1 (*6*). The SPC-based shape model provided an estimate of the asteroid spin parameters: an axis with a right ascension 96.40° ± 0.03° and declination −66.40° ± 0.03° in equinox J2000.0, and a period of 7.63262 ± 0.00002 hours. Our derived rotation period is consistent with ground-based observations, and our pole direction fits the second most probable solution compiled from ground- and space-based observations (*6*, *14*). The obliquity—the angle between Ryugu's orbital and rotational poles—is 171.64° ± 0.03°, which is close to perfectly retrograde rotation (which would be at 180°). No wobble or change of the rotation rate have been detected (*15*).

Ryugu has an oblate body, with an equatorial radius of 502 ± 2 m and polar-to–equatorial axis ratio of 0.872 ± 0.007. The total volume obtained from the SPC-based shape model is 0.377 km^3, with an uncertainty of 1.3%. We conducted a gravity measurement (*6*) during a spacecraft ballistic descent down to 0.85 km from the asteroid surface and a subsequent ballistic ascent up to

[1]Nagoya University, Nagoya 464-8601, Japan. [2]Institute of Space and Astronautical Science (ISAS), Japan Aerospace Exploration Agency (JAXA), Sagamihara 252-5210, Japan. [3]Auburn University, Auburn, AL 36849, USA. [4]University of Aizu, Aizu-Wakamatsu 965-8580, Japan. [5]Kobe University, Kobe 657-8501, Japan. [6]Research and Development Directorate, JAXA, Sagamihara 252-5210, Japan. [7]University of Tokyo, Tokyo 113-0033, Japan. [8]SOKENDAI (The Graduate University for Advanced Studies), Hayama 240-0193, Japan. [9]Hiroshima University, Higashi-Hiroshima 739-8526, Japan. [10]Tohoku University, Sendai 980-8578, Japan. [11]National Astronomical Observatory of Japan, Mitaka 181-8588, Japan. [12]Chiba Institute of Technology, Narashino 275-0016, Japan. [13]Kindai University, Higashi-Hiroshima 739-2116, Japan. [14]National Institute of Advanced Industrial Science and Technology, Tokyo 135-0064 Japan. [15]Kochi University, Kochi 780-8520, Japan. [16]Rikkyo University, Tokyo 171-8501, Japan. [17]National Institute of Information and Communications Technology, Kashima 314-8501, Japan. [18]Università d'Annunzio, 65127 Pescara, Italy. [19]Seoul National University, Seoul 08826, Korea. [20]Planetary Science Institute, Tucson, AZ 85710, USA. [21]Johns Hopkins University Applied Physics Laboratory, Laurel, MD 20723, USA. [22]Université Côte d'Azur, Observatoire de la Côte d'Azur, Centre National de la Recherche Scientifique (CNRS), Laboratoire Lagrange, 06304 Nice, France. [23]University of Colorado, Boulder, CO 80309, USA. [24]NASA Johnson Space Center, Houston, TX 77058, USA. [25]Meiji University, Kawasaki 214-8571, Japan. [26]DLR (German Aerospace Center), Institute of Space Systems, 28359 Bremen, Germany. [27]Centre National d'Etudes Spatiales (CNES), 31401 Toulouse, France. [28]DLR, Institute of Planetary Research, 12489 Berlin-Adlershof, Germany. [29]Institute d'Astrophysique Spatiale, 91405 Orsay, France. [30]DLR, Microgravity User Support Center, 51147 Cologne, Germany.
***Corresponding author. Email: seicoro@eps.nagoya-u.ac.jp** †Present address: National Institute for Environmental Studies, Tsukuba 305-8506, Japan. ‡Present address: Mitsubishi Electric Corporation, Kamakura 247-8520, Japan. §Deceased.

Downloaded from http://science.sciencemag.org/ on April 25, 2019

5.4 km (*6*). The estimated mass is 4.50×10^{11} kg, with an uncertainty of 1.3%, mainly because of uncertainties in the solar radiation pressure on the spacecraft. The bulk density is therefore 1.19 ± 0.02 g cm^{-3}, which is less than the bulk densities (1.6 to 2.4 g cm^{-3}) measured for hydrated carbonaceous asteroids (Ch- and Cgh-type) (*16*). However, it falls within the 0.8 to 1.5 g cm^{-3} range measured for BCG-types [B-, C-, Cb-, and Cg-type; Ryugu is Cb-type (*8*)], which might be related to unheated icy asteroids (*16*).

NIRS3 observations indicate that OH-bearing minerals are ubiquitous on the surface of Ryugu (*10*). The presence of water ice could explain the low bulk densities of main-belt carbonaceous asteroids but is unlikely at Ryugu because the radiative equilibrium temperature (~250 K) is higher than the ice sublimation temperature (~230 K), even at its calculated central pressure of ~8 Pa, and the estimated thermal diffusion time ($<10^5$ year) is much shorter than the typical dynamical lifetime of near-Earth asteroids ($\sim10^7$ year) (*6*).

The total porosity is derived (*6*) to be >50% if the constituent grain density is similar to those of carbonaceous chondrites, of which the lowest known is the 2.42 ± 0.06 g cm^{-3} Orgueil CI meteorite (*17*). The estimated total porosity is slightly higher than the rubble-pile asteroid Itokawa (44 ± 4%) (*6*), suggesting that Ryugu is also a rubble pile—an aggregate of numerous rocky blocks bound primarily by self-gravity, with low cohesive strength and high bulk porosity. This is consistent with the hypothesis that all SS bodies with diameters of ~1 km are rubble piles (*18*). These asteroids might have originally formed from reaccumulation of fragments generated by catastrophic disruption events of ~100-km-sized parent bodies (*19*). Ryugu's high porosity could be ascribed to loss of volatile components during or after the formation of the rubble pile, if its parent body was an icy asteroid.

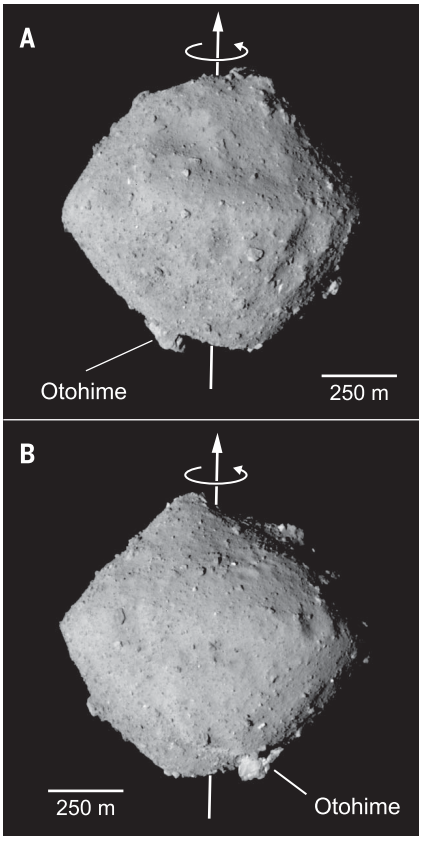

Fig. 1. Visible light images of Ryugu. Taken with ONC-T from 20 km altitude on 10 July 2018. White arrows represent the spin axis. The prime meridian is defined in (*8*). (**A**) Hemisphere centered at 5°S, 11°E (image number hyb2_onc_20180710_121100_tvf). (**B**) Hemisphere centered at 5°S, 189°E (hyb2_onc_20180710_082316_tvf).

Further evidence for a rubble-pile structure is the abundance of large boulders on the surface. The largest, Otohime, is located near the south pole and ~160 m in its longest axis (Fig. 1). The spatial density of boulders on Ryugu with longest axes >20 m is more than twice that on Itokawa (*8*). Gravitational capture of ejecta after impact cratering on this body cannot be responsible for these large boulders because their sizes are larger than the ejecta expected from even the largest crater, Urashima (~290 m in diameter) (*8*, *20*). These boulders are most likely fragments that accreted during the formation of Ryugu, after disruption of its parent body (*19*).

Little was known about Ryugu's shape before Hayabusa2's arrival because of a lack of radar imaging data and limited constraints from light curve observations (*14*). Hayabusa2 images reveal that Ryugu is a spinning top–shaped asteroid; there is an elevated ridge around the equator, from which near conical surfaces extend to the midlatitudes, with an average surface tilt angle of 34° ± 4° relative to its spin axis (Fig. 2, fig. S3, and table S2) (*6*). Ryugu's shape is similar to that of Bennu (*5*, *21*). Other spinning top–shaped near-Earth asteroids have been observed with ground-based radar (table S3). However, Ryugu's shape was unexpected because its rotation rate is slower than most of the currently known spinning top–shaped asteroids (*22*).

The aspect ratio of Ryugu's equatorial cross section is 0.96, and the circularity—the ratio of the circumference of a circle with the same area as the cross section to the perimeter—is 0.93 (table S3) (*6*). This suggests rotation-induced deformation of Ryugu, owing to a short spin period (*19*, *23*, *24*). However, the current spin rate is too slow to induce the deformation because the magnitude ratio of the centrifugal force to gravity at the equatorial radius is only ~0.2. Thus, Ryugu must have spun faster in the past and later slowed down to its current rate. This deformation hypothesis would also explain surface tilt angles that are symmetric and independent of longitude in the low latitudes (*6*, *8*). Exceptions are several crater-affected portions, which must have formed after the equatorial ridge.

To constrain the past spin rate that formed the spinning-top shape, we analyzed the distribution of surface slopes—the angle between the normal vector to the surface and that to the surface of equipotential gravitational field—at different spin rates (*21*). Assuming a uniform density distribution, we used the derived bulk density and shape to calculate the surface slope distributions (Fig. 3A) and maps (Fig. 3B). At the current rotation period, the majority of the surface has slopes <35°, with an average of 11.8°, but Ryugu exhibits latitudinal variation; the midlatitudes have lower slopes, whereas both sides of the equatorial ridge have higher slopes. This results from the surface geopotential that has local maxima in the equatorial and polar regions and becomes lowest at the midlatitudes (fig. S4). At a rotation period P_a of 4.0 hours, the local minimum moves to the equator, whereas the slopes still have latitudinal variation (fig. S5). At P_a = 3.5 hours, which is almost equal to the critical spin limit at which the centrifugal force exceeds gravity at some surface points near the equator, the surface slope distribution is centered at $31°^{+14°}_{-11°}$ (Fig. 3A). This distribution is consistent with a typical friction angle of granular materials (~35°) (*25*), suggesting topographic relaxation that homogenized the slope distribution (*8*). During this process, the variation in surface slopes minimizes at low- and midlatitudes (Fig. 3, A and B, and fig. S5) as a result of a deformation process that produced the equatorial ridge (*18*, *21*).

Geological features of the equatorial ridge (*8*) are (i) large unperturbed craters overlying the ridge, suggesting that the ridge formed before the craters; (ii) overlapped boulders, indicating surface mass wasting from the equator to the midlatitudes; and (iii) no evidence of grain-size segregation, unlike Itokawa (*4*), suggesting a lower degree of global surface activity. No structural linear features have been confirmed around the equatorial region, owing to limited lighting conditions in available high-resolution images.

To determine the material properties of the equatorial ridge, we analyzed observation data acquired for the purpose of evaluating candidate sample collection sites: four (L sites) on the equatorial ridge and three (M sites) at higher latitudes (15° to 30°) (fig. S6 and table S4) (*6*). Each candidate region has a size of 14° by 14° (about 110 by 110 m^2), which were targeted for detailed investigation. The variation between these regions in the visible and NIR reflectance data is <15%, suggesting efficient mixing processes in the surface layer (*8*, *10*). Within this limited spectral variation, a difference was found in ONC-T data on the spectral slope γ between the b- and x-bands (0.48 to 0.86 μm) (*6*, *8*). High-resolution maps of γ at candidate sampling sites reveal that bluish (lower γ) and reddish (higher γ) materials are mixed in different degrees (Fig. 4A). The slope γ was found to correlate with the v-band reflectance factor r_v (*6*, *8*). The sites along the equatorial ridge (L-sites), especially L08, have brighter bluish spectra, whereas those in higher latitudes (M-sites), especially M01, exhibit darker reddish spectra (Fig. 4B). The trend of r_v with γ may be ascribed to the effect of space exposure on fresh bright-blue materials, leading to reddening and darkening (*8*). Thus, mass wasting after spin down of Ryugu probably exposed fresh subsurface materials on the equatorial ridge.

Downloaded from http://science.sciencemag.org/ on April 25, 2019

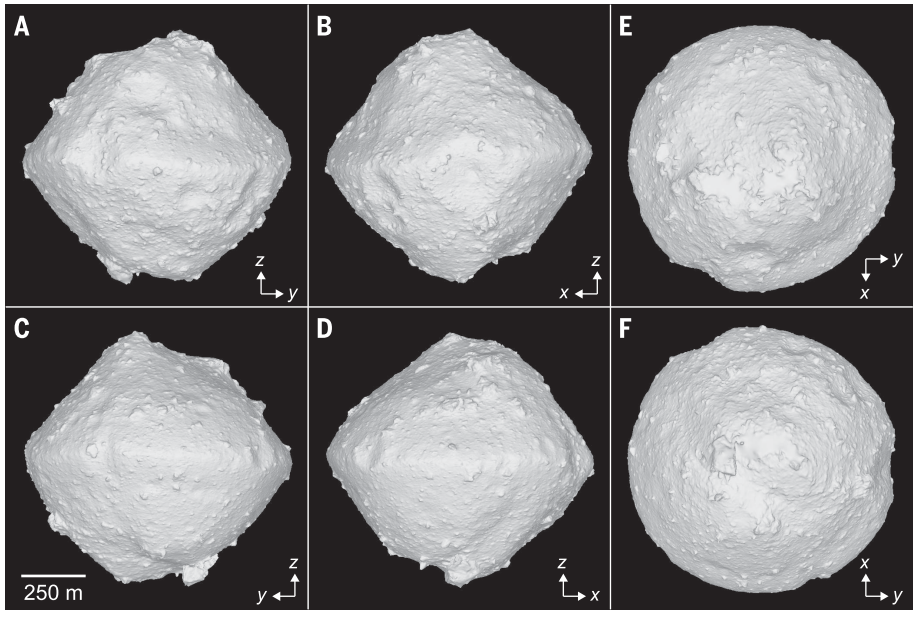

Fig. 2. Shape model of Ryugu. (**A** to **F**) The model was generate by using the SfM method with 3,145,728 facets (SFM20180804), based on 214 ONC-T images taken from 5.1 and 6.5 km altitudes. The body-fixed Cartesian coordinates (*x*, *y*, *z*) have their origin at the center of the figure, *z* along the spin axis, *x* pointing to the prime meridian, and are indicated in each image. Views are from the (A) +*x*, (B) +*y*, (C) −*x*, (D) −*y*, (E) +*z*, and (F) −*z* directions.

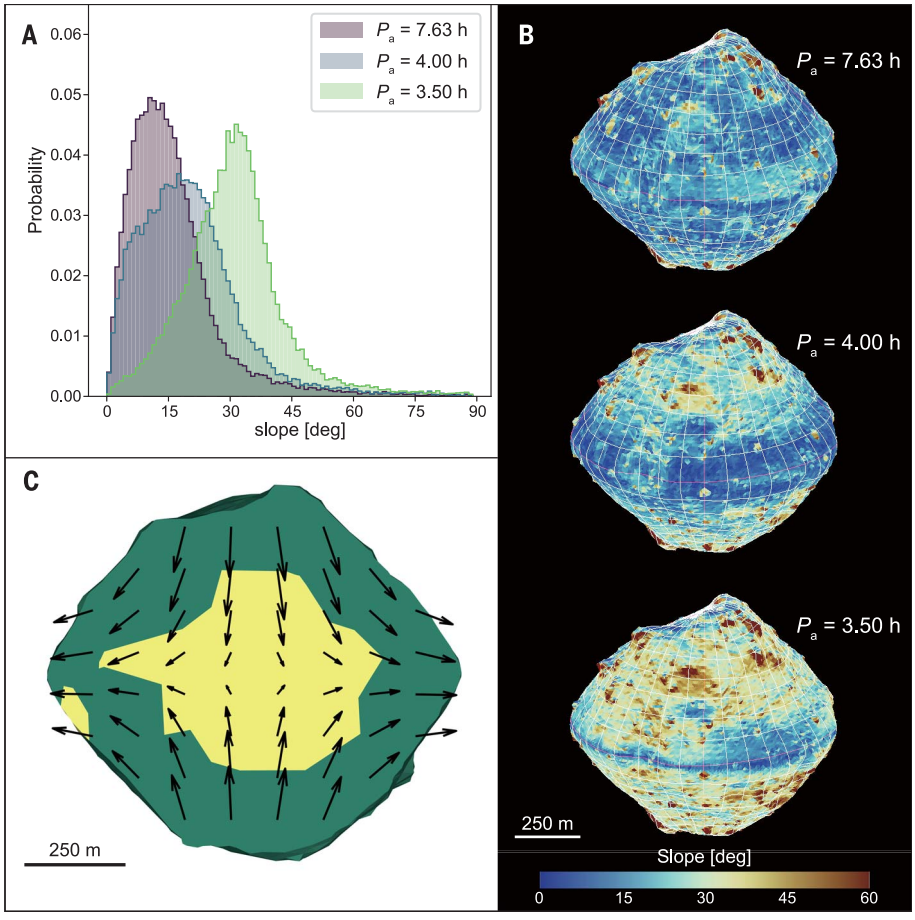

Fig. 3. Slope distribution and failure mode analysis. Reduced versions of SfM-based [(A) and (B), 49,152 facets] and SPC-based [(C), 3072 facets] shape models were used. The density is assumed to be constant at 1.2 g cm^{-3}. (**A**) Area-weighted slope distribution at spin periods of 7.63, 4.0, and 3.5 hours. (**B**) Slope maps projected onto the shape model at different spin periods. (**C**) Failed region (yellow) and deformation vectors on the meridional cross-section viewed from a longitude of 30°E at a spin period of 3.5 hours. The minimum cohesive strength to keep the original shape is ~4 Pa.

Our current observations are insufficient to identify when and how the spinning-top shape formed. Possible timings are either an early reaccumulation stage after catastrophic disruption of Ryugu's parent body (*19*) and/or a later stage due to quasi-static rotational acceleration (*23*, *24*). Early-stage formation may explain the presence of large craters on the equatorial ridge. However, the conditions for producing a spinning-top shape are unclear because Ryugu would need to gain a high-enough angular momentum during reaccumulation to produce its axisymmetric shape and circular ridge but avoid a nonaxisymmetric rotational instability that makes the shape elongated (*26*).

In the later stage, the Yarkovsky-O'Keefe-Radzievskii-Paddack (YORP) effect—a radiation recoil torque affecting the rotation state of a small asteroid—is responsible for the quasi-static acceleration of asteroids (*18*). When a spheroidal asteroid spins rapidly, strong centrifugal forces may induce deformation processes either on the surface (*23*, *27*) or in the interior (*28*, *29*), depending on the internal structure (*29*, *30*). The large porosity of Ryugu, the dominance of large grains (>1 cm) across its surface (*8*), and the lack of observed flat floors in its largest craters (*8*) suggest that the internal cohesive strength of the asteroid may be uniform and low.

Given the bulk density, shape, and uniform structure, we calculated the failure mode of Ryugu by using a plastic finite element model (FEM) technique (*6*, *22*). This FEM method models continuum media to describe irreversible deformation of the regolith in asteroids. If Ryugu rotates at P_a < 3.75 hours, tension plays a dominant role in deformation in the interior (fig. S7). At P_a = 3.5 hours, the first structural failure occurs in the central region (Fig. 3C) if the cohesive strength (*31*) is uniformly ~4 Pa, which is similar to the predicted cohesive strength of small bodies (*24*, *28*). Whereas the van der Waals force may

Downloaded from http://science.sciencemag.org/ on April 25, 2019

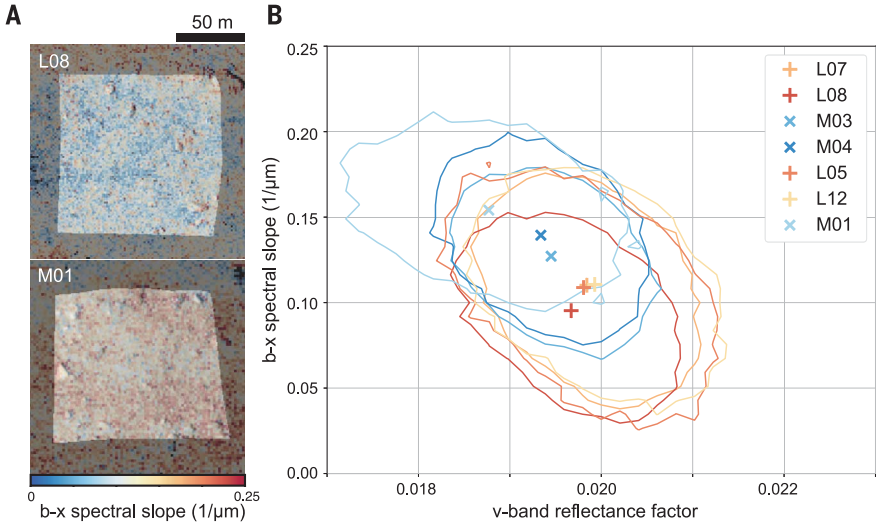

Fig. 4. Visible spectral properties of candidate sampling sites. In accordance with a safety index (fig. S6) (*6*), we chose seven candidate sampling sites—L05, L07, L08, L12, M01, M03, and M04—where L and M indicate low-latitude and midlatitude (15° to 30°) regions, respectively. (**A**) ONC-T v-band images of two representative candidate sites, L08 (top, hyb2_onc_20180801_141045_tvf) and M01 (bottom, hyb2_onc_20180801_172245_tvf), from altitude of ~5 km, overlain with color maps of the b-x (0.48 to 0.86 μm) spectral slope. (**B**) Spectral slope and reflectance factor (*6*) in the v-band for the seven candidate landing sites. Symbols (L, +; M, ×) and lines indicate the median values and 1σ variations inside those sites, respectively (*6*).

contribute to cohesion (*24*), density inhomogeneity or particle interlocking may also produce equivalent mechanical strength. The failed region spreads over the interior, driving outward radial deformation parallel to the equatorial plane and inward vertical deformation around the spin axis (Fig. 3C). This model may support a lower degree of global surface activity on Ryugu (*8*). However, we do not rule out contributions from surface landslides to spinning top–shape formation (*29*), which can be driven by local heterogeneities (*15*) or a gradual increase in strength of the asteroid with depth. These scenarios predict differing freshness of the subsurface material beneath the equatorial ridge because of the time available for space weathering.

In situ surface data that enable the assessment of possible material contrasts between the equatorial ridge and midlatitudes was obtained by a lander. The Mobile Asteroid Surface Scout (MASCOT) (*32*, *33*) landed in a midlatitude region on Ryugu on 3 October 2018. On the basis of these assessments, we selected a potential landing site (L08) (fig. S6) on the equatorial ridge to perform material sampling, with the goal of constraining the evolution of this spinning top–shaped asteroid.

REFERENCES AND NOTES

1. C. M. O. Alexander *et al.*, *Science* **337**, 721–723 (2012).
2. S. Tachibana *et al.*, *Geochem. J.* **48**, 571–587 (2014).
3. S. Watanabe *et al.*, *Space Sci. Rev.* **208**, 3–16 (2017).
4. A. Fujiwara *et al.*, *Science* **312**, 1330–1334 (2006).
5. D. S. Lauretta *et al.*, *Space Sci. Rev.* **212**, 925–984 (2017).
6. Materials and Methods are available as supplementary materials.
7. S. Kameda *et al.*, *Space Sci. Rev.* **208**, 17–31 (2017).
8. S. Sugita *et al.*, *Science* **364**, eaaw0422 (2019).
9. T. Okada *et al.*, *Space Sci. Rev.* **208**, 255–286 (2017).
10. K. Kitazato *et al.*, *Science* **364**, 272–275 (2019).
11. T. Mizuno *et al.*, *Space Sci. Rev.* **208**, 33–47 (2017).
12. R. W. Gaskell *et al.*, *Meteorit. Planet. Sci.* **43**, 1049–1061 (2008).
13. R. Szeliski, *Computer Vision: Algorithms and Applications* (Springer, 2010).
14. T. G. Müller *et al.*, *Astron. Astrophys.* **599**, A103 (2017).
15. A small deviation (0.7° to 0.8°) of the principal axis of inertia from the spin axis was obtained, considering the shape models and assuming uniform density distribution (*6*).
16. P. Vernazza *et al.*, *Astrophys. J.* **806**, 204 (2015).
17. R. J. Macke, G. J. Consolmagno, D. T. Britt, *Meteorit. Planet. Sci.* **46**, 1842–1862 (2011).
18. K. J. Walsh, *Annu. Rev. Astron. Astrophys.* **56**, 593–624 (2018).
19. P. Michel, W. Benz, P. Tanga, D. C. Richardson, *Science* **294**, 1696–1700 (2001).
20. T. Michikami *et al.*, *Earth Planets Space* **60**, 13–20 (2008).
21. D. J. Scheeres *et al.*, *Icarus* **276**, 116–140 (2016).
22. M. Hirabayashi, D. J. Scheeres, *Icarus* **317**, 354–364 (2019).
23. K. J. Walsh, D. C. Richardson, P. Michel, *Nature* **454**, 188–191 (2008).
24. P. Sánchez, D. J. Scheeres, *Icarus* **271**, 453–471 (2016).
25. T. W. Lambe, R. V. Whitman, *Soil Mechanics* (Wiley, 1969).
26. S. Chandrasekhar, Ellipsoidal Figures of Equilibrium (Yale Univ. Press, 1969).
27. D. J. Scheeres, *Icarus* **247**, 1–17 (2015).
28. M. Hirabayashi, D. J. Scheeres, *Astrophys. J.* **798**, L8 (2014).
29. M. Hirabayashi, D. P. Sánchez, D. J. Scheeres, *Astrophys. J.* **808**, 63 (2015).
30. Y. Zhang *et al.*, *Astrophys. J.* **857**, 15 (2018).
31. The cohesive strength σ_c of Ryugu-formed aggregates is given by $\sigma_c = \sigma_t \tan\theta$, where σ_t and θ are the tensile strength and the angle of friction of the aggregates, respectively.
32. R. Jaumann *et al.*, *Space Sci. Rev.* **208**, 375–400 (2017).
33. J.-P. Bibring *et al.*, *Space Sci. Rev.* **208**, 401–412 (2017).

ACKNOWLEDGMENTS

The Hayabusa2 spacecraft was developed and built under the leadership of JAXA, with contributions from the German Aerospace Center (DLR) and the Centre National d'Études Spatiales (CNES), and in collaboration with Nagoya University, University of Tokyo, National Astronomical Observatory of Japan, University of Aizu, Kobe University, and other universities, institutes, and companies in Japan. We thank NASA, DSN, and JPL for their support for the execution of the Hayabusa2 mission and Hayabusa2 Joint Science Team members for fruitful science discussions. We also thank the many engineers who have contributed to the success of the Hayabusa2 mission, especially T. Masuda, S. Yasuda, K. Matsushima, and T. Ohshima at NEC Corporation. S.W. thanks C. M. Ernst for her support of the development of the SPC-based shape model. T.N. thanks to K. Amano, H. Mita, and S. Kobayashi for their support of the LSS process. M.Hi. acknowledges the use of ANSYS Mechanical APDL (18.1), which is licensed by Samuel Ginn College of Engineering at Auburn University. **Funding:** This study was supported by KAKENHI from the Japan Society for the Promotion of Science (JSPS) (grants JP17H06459, JP17K05639, JP16H04059, JP17KK0097, JP26287108, JP16H04044, and JP16H04044), the JSPS Core-to-Core program "International Network of Planetary Sciences", and the National Institutes of Natural Sciences (AB302006). O.S.B. acknowledges funding support from NASA New Frontier Program (NNM10AA11C). P.M. acknowledges funding support from the French space agency CNES. **Author contributions:** Conceptualization: S.W., M.Hi., N.H. (Aizu), and Y.Ii. Spacecraft operation and data acquisition: M.Yo, S.Ki., H.T., T.O., M.Ab., Y.Ya., S.Tan. (JAXA), K.S., M.Ya, T.Y., N.O., G.O., Y.M., K.Yoshik., T.T., Y.Ta., A.F., C.Hi, T.I., M.Ha., S.H., O.M., H.Sa., T.Sh., S.So., H.Yan., R.T., M.O., K.O., F.T., T.Sa., S.N., and Y.Ts. Analysis (shape models): S.W., M.Hi., N.H. (Aizu), N.H. (Kobe), R.N., Y.S., Y.Is., K.M., H.T., S.Su., R.G., E.P., O.S.B., Y.Ya, S.Tan. (Kobe), N.Ni., T.Su., and T.Y. Analysis (gravity): H.I., M.Yo., A.S.F., J.W.M., D.J.S., Y.M., K.Yoshik., S.So., and Y.Ts. Analysis (ephemeris): H.T. Analysis (LSS): S.W., E.T., S.Ki., H.Yab., T.N., S.Tac., Y.Is., T.Mo., K.K., N.S., K.M., K.W., H.Se., C.Ho., T.Mi., T.K., R.Ho., S.Ka., T.F., H.M., G.K., P.M., P.A.A., S.Tan. (JAXA), M.M., Y.Yo., H.Su., K.Yoshio., Y.C., H.K., and R.He. Project administration: S.W., M.Yo., S.Tac., K.K., S.Su., T.O., N.Na., M.Ar., M.Ab., S.T. (JAXA), M.F., T.-M.H., A.M., R.J., J.-P.B., C.K., F.T., T.Sa., S.N., and Y.Ts. Writing: S.W., M.Hi., N.H. (Aizu), R.N., Y.S., H.I., E.T., S.Ki., T.N., S.Tac., K.W., H.T., T.K., G.K., O.S.B., P.M., D.J.S., P.A.A., and S.So. All authors discussed the results and commented on the manuscript. **Competing interests:** Y.Ya. is also affiliated with Tokyo Metropolitan University. **Data and materials availability:** All images, the shape model, and original software presented in this paper are available at the JAXA Data Archives and Transmission System (DARTS) at www.darts.isas.jaxa.jp/pub/hayabusa2/paper/Watanabe_2019. Additional data from the mission will be delivered to the DARTS archive at www.darts.isas.jaxa.jp/planet/project/hayabusa2, and higher-level data products will be available in the Small Bodies Node of the Planetary Data System at https://pds-smallbodies.astro.umd.edu 1 year after departure from the asteroid. Distribution of the SPC software is legally restricted by the U.S. International Traffic in Arms Regulation. U.S. citizens (only) may request an SPC research license, with appropriate restrictions, at http://spc.psi.edu. For our FEM analysis, the input files to ANSYS Mechanical APDL are available at http://hdl.handle.net/11200/49368.

SUPPLEMENTARY MATERIALS

science.sciencemag.org/content/364/6437/268/suppl/DC1
Materials and Methods
Figs. S1 to S7
Tables S1 to S4
References (*34*–*60*)

29 October 2018; accepted 7 March 2019
Published online 19 March 2019
10.1126/science.aav8032

Downloaded from http://science.sciencemag.org/ on April 25, 2019

Science

Hayabusa2 arrives at the carbonaceous asteroid 162173 Ryugu—A spinning top–shaped rubble pile

S. Watanabe, M. Hirabayashi, N. Hirata, Na. Hirata, R. Noguchi, Y. Shimaki, H. Ikeda, E. Tatsumi, M. Yoshikawa, S. Kikuchi, H. Yabuta, T. Nakamura, S. Tachibana, Y. Ishihara, T. Morota, K. Kitazato, N. Sakatani, K. Matsumoto, K. Wada, H. Senshu, C. Honda, T. Michikami, H. Takeuchi, T. Kouyama, R. Honda, S. Kameda, T. Fuse, H. Miyamoto, G. Komatsu, S. Sugita, T. Okada, N. Namiki, M. Arakawa, M. Ishiguro, M. Abe, R. Gaskell, E. Palmer, O. S. Barnouin, P. Michel, A. S. French, J. W. McMahon, D. J. Scheeres, P. A. Abell, Y. Yamamoto, S. Tanaka, K. Shirai, M. Matsuoka, M. Yamada, Y. Yokota, H. Suzuki, K. Yoshioka, Y. Cho, S. Tanaka, N. Nishikawa, T. Sugiyama, H. Kikuchi, R. Hemmi, T. Yamaguchi, N. Ogawa, G. Ono, Y. Mimasu, K. Yoshikawa, T. Takahashi, Y. Takei, A. Fujii, C. Hirose, T. Iwata, M. Hayakawa, S. Hosoda, O. Mori, H. Sawada, T. Shimada, S. Soldini, H. Yano, R. Tsukizaki, M. Ozaki, Y. Iijima, K. Ogawa, M. Fujimoto, T.-M. Ho, A. Moussi, R. Jaumann, J.-P. Bibring, C. Krause, F. Terui, T. Saiki, S. Nakazawa and Y. Tsuda

Science **364** (6437), 268-272.
DOI: 10.1126/science.aav8032originally published online March 19, 2019

Hayabusa2 at the asteroid Ryugu

Asteroids fall to Earth in the form of meteorites, but these provide little information about their origins. The Japanese mission Hayabusa2 is designed to collect samples directly from the surface of an asteroid and return them to Earth for laboratory analysis. Three papers in this issue describe the Hayabusa2 team's study of the near-Earth carbonaceous asteroid 162173 Ryugu, at which the spacecraft arrived in June 2018 (see the Perspective by Wurm). Watanabe *et al.* measured the asteroid's mass, shape, and density, showing that it is a "rubble pile" of loose rocks, formed into a spinning-top shape during a prior period of rapid spin. They also identified suitable landing sites for sample collection. Kitazato *et al.* used near-infrared spectroscopy to find ubiquitous hydrated minerals on the surface and compared Ryugu with known types of carbonaceous meteorite. Sugita *et al.* describe Ryugu's geological features and surface colors and combined results from all three papers to constrain the asteroid's formation process. Ryugu probably formed by reaccumulation of rubble ejected by impact from a larger asteroid. These results provide necessary context to understand the samples collected by Hayabusa2, which are expected to arrive on Earth in December 2020.

Science, this issue p. 268, p. 272, p. 252; see also p. 230

ARTICLE TOOLS http://science.sciencemag.org/content/364/6437/268

SUPPLEMENTARY MATERIALS http://science.sciencemag.org/content/suppl/2019/03/18/science.aav8032.DC1

RELATED CONTENT http://science.sciencemag.org/content/sci/364/6437/272.full
http://science.sciencemag.org/content/sci/364/6437/eaaw0422.full
http://science.sciencemag.org/content/sci/364/6437/230.full

REFERENCES This article cites 47 articles, 5 of which you can access for free
http://science.sciencemag.org/content/364/6437/268#BIBL

Use of this article is subject to the Terms of Service

Science (print ISSN 0036-8075; online ISSN 1095-9203) is published by the American Association for the Advancement of Science, 1200 New York Avenue NW, Washington, DC 20005. 2017 © The Authors, some rights reserved; exclusive licensee American Association for the Advancement of Science. No claim to original U.S. Government Works. The title *Science* is a registered trademark of AAAS.

Downloaded from http://science.sciencemag.org/ on April 25, 2019

PERMISSIONS http://www.sciencemag.org/help/reprints-and-permissions

Downloaded from http://science.sciencemag.org/ on April 25, 2019

Use of this article is subject to the Terms of Service

Science (print ISSN 0036-8075; online ISSN 1095-9203) is published by the American Association for the Advancement of Science, 1200 New York Avenue NW, Washington, DC 20005. 2017 © The Authors, some rights reserved; exclusive licensee American Association for the Advancement of Science. No claim to original U.S. Government Works. The title *Science* is a registered trademark of AAAS.